J. Fluid Mech. (1984), *vol.* 143, *pp.* 305–326
Printed in Great Britain

Shock structure near a wall in pure inert gas and in binary inert-gas mixtures

By B. SCHMIDT, F. SEILER AND M. WÖRNER

Institut für Strömungslehre und Strömungsmaschinen, Universität Karlsruhe, F.R.G.

(Received 2 June 1983)

The shock-wave structure close to a wall in pure argon and binary mixtures of noble gases (argon–helium, xenon–helium) is investigated experimentally and numerically in the shock-wave Mach-number range $2.24 \leqslant M_s \leqslant 9.21$. Measured and calculated density profiles are compared, and some conclusions are drawn about the accommodation at the wall and the intermolecular force potential.

For binary gas mixtures only a few results are presented. Weak argon signals of the electron-beam-luminescence method on the experimental side and the computer time needed for the numerical simulation allowed the treatment of a few parameter combinations only.

1. Introduction

A shock wave, moving along an infinite wall, develops a two-dimensional structure with large gradients in the macroscopic quantities (density, pressure, temperature and flow velocity) close to the wall. Figure 1 shows a sketch of the flowfield of interest, the 'foot region' of a shock wave. Experimental data for pure argon have been collected for shock Mach numbers of $M_s = 2.24$, 3.55, 6.46 and 9.21. The density has been measured with a multibeam laser differential interferometer. These data are compared with numerical results of the direct simulation Monte Carlo method as developed by Bird (1976).

The success of the simulation method and the large gradients in the flow variables observed gave the motivation to extend the investigation of the shock 'foot region' to binary inert-gas mixtures.

2. Numerical approach (theory)

The characteristic length of the problem is the shear-layer thickness δ (see figure 1) at the downstream side of the shock wave. δ is of the order of one mean free path length λ_1 (the subscript 1 designates the undisturbed region upstream of the shock wave). The flow within this region lies between the transition and free molecular flow. A gaskinetic theory or calculation method must be used to describe the flow. Here the direct-simulation Monte Carlo method, a numerical approach to rarefied gas flows, as developed by Bird (1976), has been applied with success (Seiler & Schmidt 1979, 1981; Seiler 1980).

The physical model used for simulation of the flow of interest is shown in figure 2. The computed flow field is bounded by a piston, a centreline, a left border (endwall) and the solid wall. The flowfield is subdivided into about 1800 cells, and each cell contains $N = 6$ model molecules at the start of a computer run. The size of a cell is such that the change of the flow properties over the cell is small. The cell extension

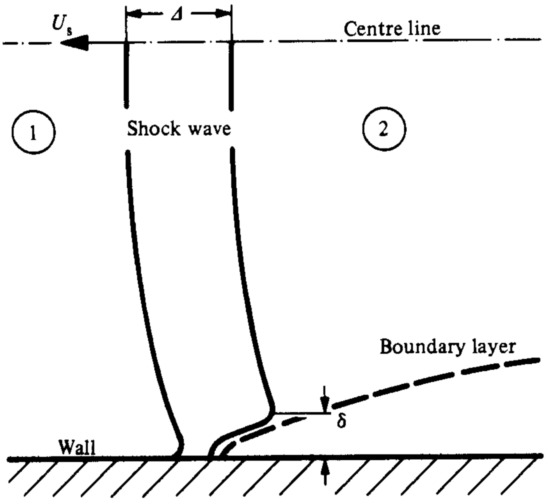

FIGURE 1. Flow field of interest; $\varDelta$ = shock-wave thickness, δ = shear-layer thickness at the downstream end of the shock wave.

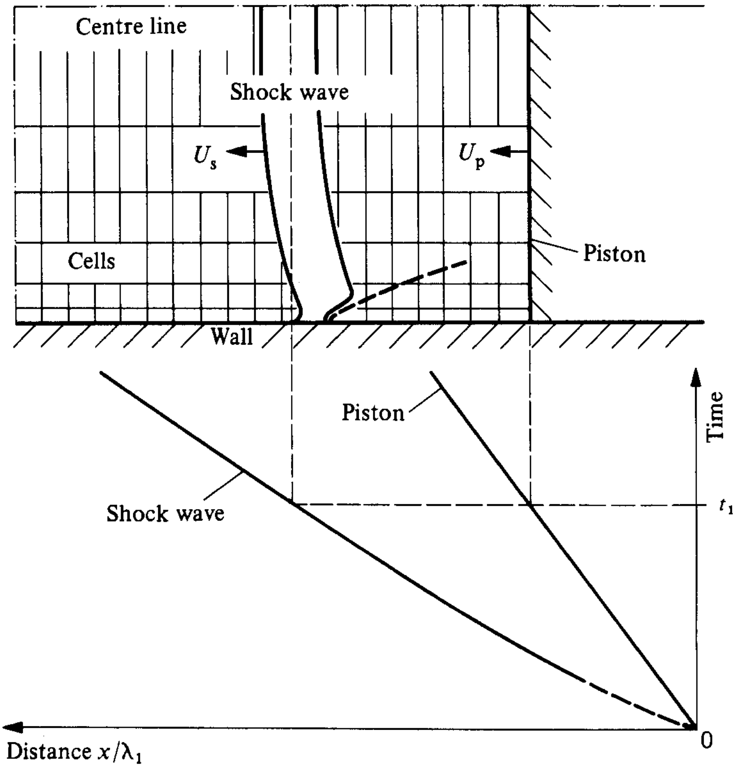

FIGURE 2. Shock-wave model for numerical simulation and time–distance plot.

in the x-direction is about $0.51\text{–}1.0\lambda_1$ for all cells, and increases in the y-direction inversely proportionally to the gradient in the state variables from $0.1\lambda_1$ at the wall to about $10\lambda_1$ at the centreline.

At the start of a simulation computer run the molecules are distributed equally over each cell with a Maxwellian velocity distribution, representing T_1. The simulation proceeds in discrete time steps Δt and the molecules move with their individual velocities. At the solid wall the molecules are reflected according to the wall accommodation coefficient α. At the other three boundaries the molecules are subject to specular reflection ($\alpha = 0$).

After each Δt, in each cell such a number of collision pairs are selected randomly according to their relative speed g, until the sum of the collision times $\Sigma\Delta t_{\text{coll}}$ reaches Δt. Δt_{coll} is inversely proportional to the relative speed g of the selected colliding pair and to the square of the number of molecules in the cell, N^2. The collision process is calculated in the classical way, using an appropriate intermolecular force potential ϕ (pure repulsive inverse-power force potential $\phi \sim r^{-\nu}$ with $5 \leqslant \nu \leqslant \infty$; $\nu = 5$ very soft (Maxwell) potential; $\nu = 10$ close to the repulsive part of a real potential for temperatures reached in shock waves as investigated in this work; $\nu = \infty$ hard-sphere model, Lennard-Jones (12-6) potential $\phi = 4\epsilon[(\sigma/r)^{12} - (\sigma/r)^6]$, $\epsilon =$ potential well depth, $r =$ distance between colliding gas particles, $r = \sigma$ gives $\phi = 0$). If a gas particle crosses a cell border to a cell of different size, the change in the cell size must be considered by production or destruction of gas particles proportional to the change of the cell size. By sampling after a sufficient number of time intervals Δt over appropriate molecular quantities within each cell, the macroscopic flow quantities, density, pressure, temperature and flow velocity, can be calculated. The limited number of molecules per cell causes a scattering of the points that represent the sampling results for the individual cells. The scattering can be reduced by averaging over $S = 10\text{–}100$ repeated computer runs. The typical final statistical scatter of Monte Carlo results is eliminated by fairing curves through the sampling points of the individual cells.

3. Experiments

The experiments have been done in a low-density shock tube of 150 mm inner diameter with a square test section of 90 × 90 mm at the end of the driven section (see figure 17). The density has been measured with a multibeam laser differential interferometer. Four interferometers were stacked perpendicular to an inserted flat plate at the test-section bottom with distances from the plate of 0.15–1.5 mm (for more details see Seiler & Schmidt 1981; Seiler 1980). The interferometer beams were focused in the test section to an effective beam diameter of 0.19 mm. The distance between the beams of each interferometer was 3.3 mm. This arrangement provided sufficient resolution in time and space for the density measurements with an initial test-gas pressure of $p_1 = 13.3\ \text{N/m}^2$. For an estimation of the influence of the flow non-uniformity in the direction of the light on the measured average density, three-dimensional results, calculated with an averaging similar to the experiment, have been compared with corresponding two-dimensional numerical-simulation results (Seiler & Schmidt 1981). The differences are small and are well within the error bars of the measured density profiles.

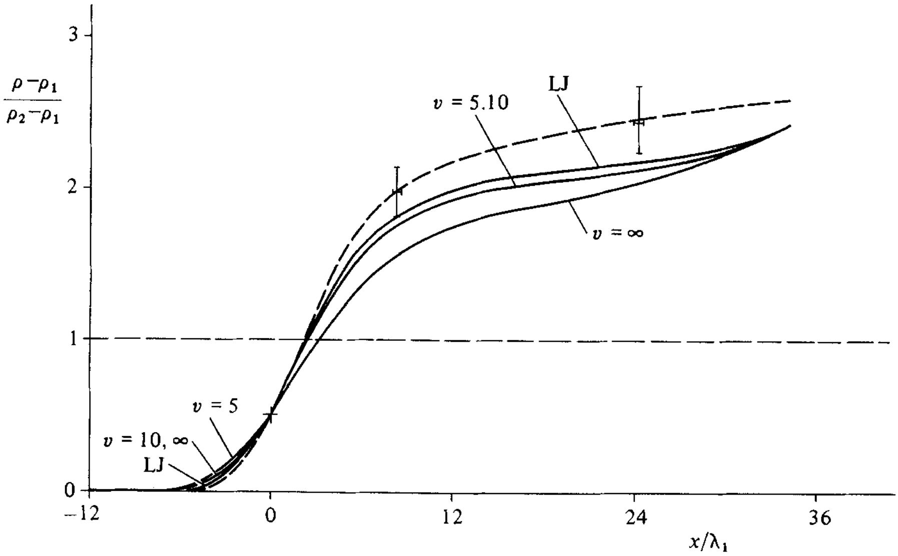

FIGURE 3. Experimental and numerical density profiles in argon; wall distance $y/\lambda_1 = 0.28$, $p_1 = 13.3$ N/m², $M_s = 2.24$, aluminium wall, $\alpha = 1.0$: ----; experiment; ——, simulation calculation, different intermolecular potentials.

4. Results

The results of simulation computer runs are compared with those of experiments in argon for shock Mach numbers of 2.24, 3.55, 6.46 and 9.21. For full accommodation at the wall ($\alpha = 1.0$) and Lennard–Jones 12-6 intermolecular force potential it is found that for $M_s = 2.24$ and 3.55, and the most sensitive density profile close to the wall with $y/\lambda_1 = 0.28$ (y = ordinate of the cell centre), the experimental density profiles are above the numerical simulation results (figure 3). For $M_s = 6.46$ and 9.21 the experimental density profiles are below the numerical simulation results (figure 4). The profiles for $M_s = 3.55$ and 6.46 are not shown.

The relative location of the experimental density profiles to the calculated ones is for $M_s = 3.55$ similar to the arrangement in figure 3 and for $M_s = 6.46$ it is similar to that in figure 4, only the differences are less pronounced. The agreement between measured and calculated density profiles can be improved for $M_s = 9.21$ (figure 4) by lowering the accommodation from full accommodation with $\alpha = 1$ to $\alpha < 1$. An α in the range $0.85 < \alpha < 0.95$ will reduce optimally the differences. The best fit to the whole shape of the experimental density profile for $M_s = 9.21$ will be given by the Lennard–Jones (12-6) intermolecular force potential (LJ in figure 4). For the weaker shock waves with $M_s = 2.24$ (figure 3) and 3.55, the agreement between experiment and simulation calculation can't be improved by changing the accommodation coefficient α. Here $\alpha > 1$ would be needed, which is physically not possible. To reduce the differences between measurement and simulation calculation in figure 3, a change in the repulsive term $(\sigma/r)^{\nu}$ with $\nu = 12$ in the Lennard–Jones (12-6) intermolecular-force potential to a weaker one with $\nu < 12$, combined with an unchanged term of attraction $(\sigma/r)^6$, will shift the calculated density profile in the right direction. It is interesting to note in figure 3 that the shift of the calculated density profiles for a pure repulsive-force potential $\phi \sim r^{-\nu}$ with $5 \leqslant \nu \leqslant \infty$ (very weak to very hard) is

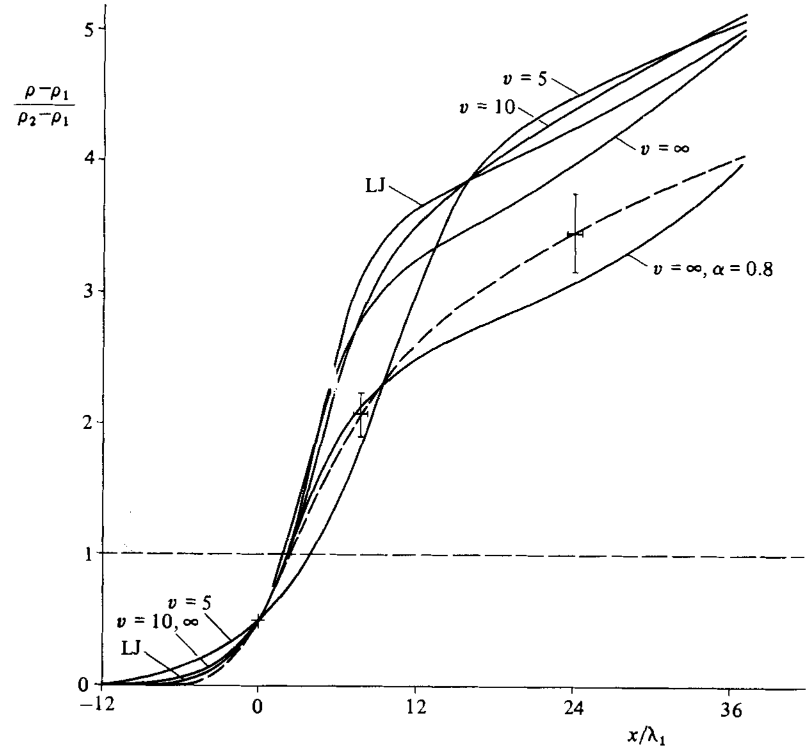

FIGURE 4. Experimental and numerical density profiles in argon; wall distance $y/\lambda_1 = 0.28$, $p_1 = 13.3\ \mathrm{N/m^2}$, $M_s = 9.21$, aluminium wall, $\alpha = 1.0$ (0.8): -----, experiment; ——, simulation calculation, different intermolecular potentials.

not sufficient to come downstream of $x/\lambda \approx 5$ above the density profile calculated with the Lennard-Jones (12-6) potential. Responsible for this fact is the influence of the attraction term in the Lennard-Jones (12-6) intermolecular-force potential.

For the next row of cells with distance of the cell centre from the wall of $y/\lambda = 1.04$, the increase of the density within and downstream of the shock wave is much less than that of the cell row at the wall $y/\lambda_1 = 0.28$ (no figure). At $y/\lambda_1 = 1.04$ the differences between measured and calculated density profiles are much smaller, too.

In figure 5 BGK (Bhatnagar-Gross-Krook) model results for $M_s = 3.55$ in argon are compared with data of the numerical-simulation method and the experiment (Gajewski & Schmidt 1980). The differences between these three density profiles are large. It must be considered, however, that the BGK model density profiles are calculated for $y/\lambda_1 = 0$ and $y/\lambda_1 = 0.56$, whereas numerical simulation and experiment produce density profiles that are density averages over a certain $\Delta y/\lambda_1$. Δy is given by the cell height or by the effective diameter of the interferometer light beam in the test section. Moreover, the BGK model shows a larger gradient $\partial\rho/\partial x$ in the shock wave than the simulation calculation or the experiment. An explanation for this difference is not known. The BGK density profiles level off to a constant value downstream of the shock wave. The influence of the developing boundary layer, having a negative displacement, is not considered.

The influence of the shock strength on the measured density profile for the cell row closest to the wall ($y/\lambda_1 = 0.28$) is shown in figure 6. With increasing shock strength

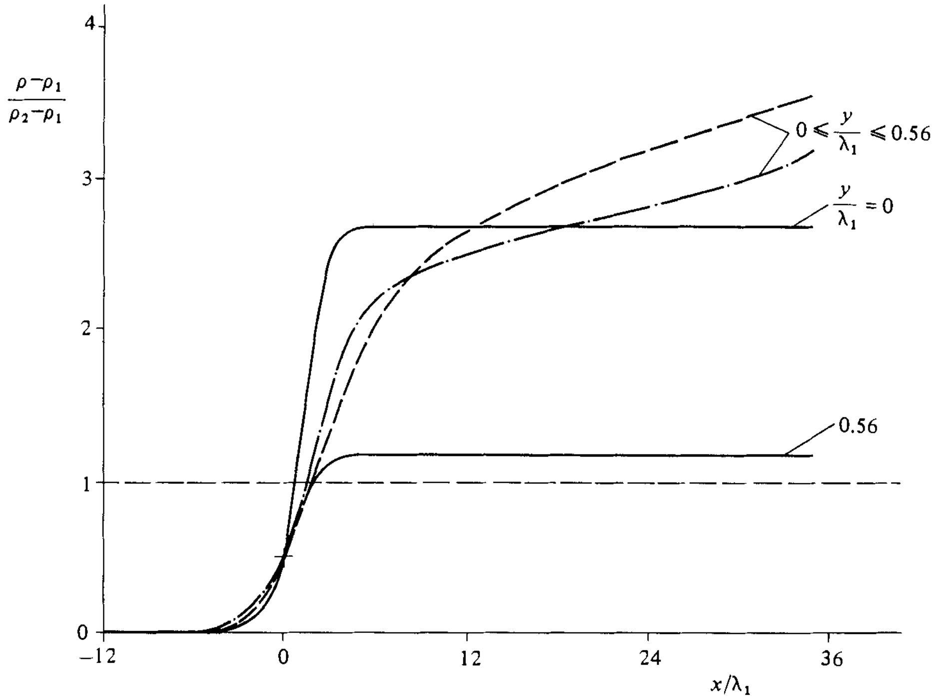

FIGURE 5. BGK model result compared with measured and calculated (simulation) density profiles in argon; $p_1 = 13.3\ \mathrm{N/m^2}$, aluminium wall, $\alpha = 1.0$; -----, experiment; –·–·–, simulation LJ (12-6) intermolecular potential, $\alpha = 1.0$; ——, BGK model (Gajewski 1980), $M_s = 3.55$.

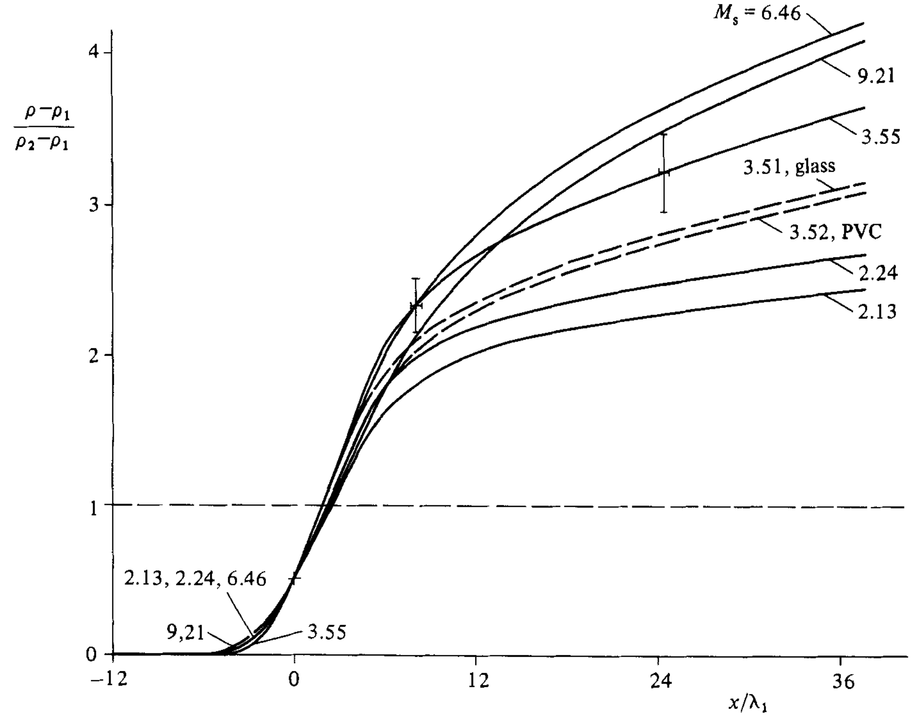

FIGURE 6. Measured density profiles in argon, different wall materials; $y/\lambda_1 = 0.28$, $p_1 = 13.3\ \mathrm{N/m^2}$: ——, aluminium wall; -----, glass or PVC wall.

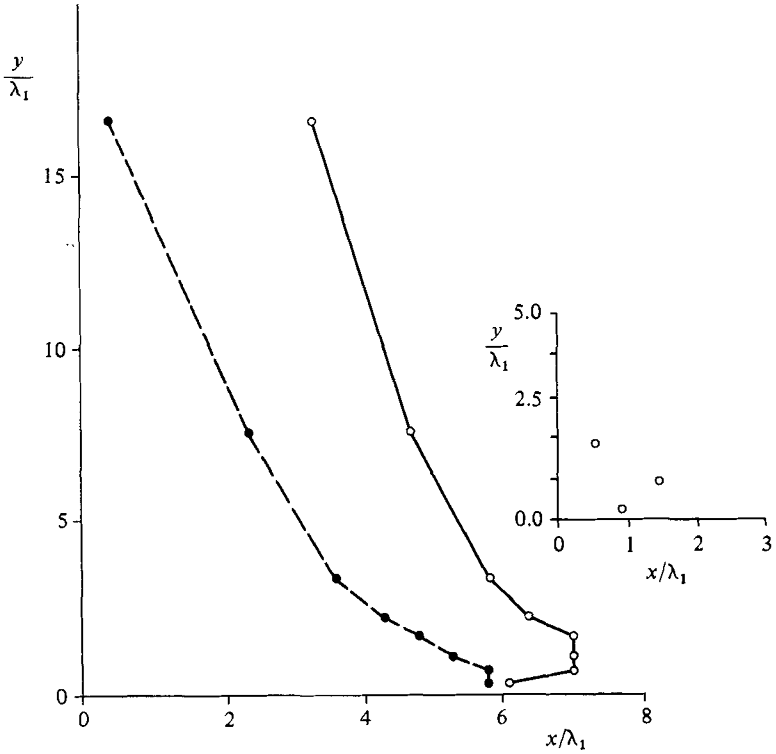

FIGURE 7. Shock-wave front curvature close to a wall: ----, temperature front, $T/T_1 = 1.04$; ——, density front $(\rho-\rho_1)/(\rho_2-\rho_1) = 0.02$, $M_s = 3.55$, $\frac{1}{2}H = 73.4$. Insert graph: experimental result, $p_1 = 13.3\ \mathrm{N/m^2}$, $(\rho-\rho_1)/(\rho_2-\rho_1) = 0.02$, $M_s = 3.55$.

(from $M_s = 2.13$ to 6.46), the density profiles rise to higher density values at the same location x/λ_1, except for the density profile for $M_s = 9.21$, which drops below the density profile for $M_s = 6.46$, indicating a less complete accommodation ($\alpha < 1$). This result supports the conclusions drawn in connection with a comparison of the calculated density profile for $M_s = 9.21$ with the measured one (figure 4).

Experimental results found with different wall materials are also shown in figure 6. For almost the same shock Mach number, the increase in density for the profile $y/\lambda_1 = 0.28$, is about the same for glass and PVC (polyvinyl-chloride), but differs considerably for the otherwise used aluminium plate. The surface of the aluminium plate was superfinished, the glass and the PVC surfaces were smooth due to the manufacturing process. All surfaces were cleaned to high vacuum condition standards.

Another interesting result has been found for the shock front curvature close to the wall. As can be seen in figure 7, the simulation calculation and the experiment produce a density front of the shock wave with a forward bend within roughly one mean free path λ_1 from the wall. But no such forward bend develops for the calculated temperature front of the shock wave. This observation can be explained by the model, in that faster gas particles (those with higher temperature) penetrate the shock front from behind and develop a temperature front, like that calculated numerically, ahead of the density front. Close to the wall these faster gas particles are cooled (slowed down) either by collision with gas particles coming directly from the colder wall or

Mach number M_s	Mixture ratio Ar/He (%/%)	Number of particles per cell and component N	Average computing time (IBM 370) per simulation run with $N = 160$ (h)
2.0	3/97	5, 10, 20, 40, 80, 160	1.1
	10/90	5, 10, 20, 40, 80, 160	1.2
	20/80	40, 80, 160	1.0
	30/70	5, 10, 20, 40, 80, 160	0.9
	50/50	40, 80, 160	0.7
	70/30	5, 10, 20, 40, 80, 160	0.8
	90/10	5, 10, 20, 40, 80, 160	0.9
	97/3	5, 10, 20, 40, 80, 160	0.9
3.5	3/97	4, 20, 40, 80, 160	1.5
	10/90	4, 10, 20, 40, 80, 160	1.9
	20/80	40, 80, 160	1.8
	30/70	4, 20, 40, 80, 160	1.6
	50/50	5, 10, 15, 20, 40, 80, 160	1.2
	70/30	4, 20. 40, 80, 160	1.1
	90/10	4, 10, 20, 40, 80, 160	1.1
	97/3	4, 20, 40, 80, 160	1.1
6.0	3/97	40, 80, 160	1.8
	10/90	5, 10, 20, 40, 80, 160	1.8
	20/80	40, 80, 160	1.8
	30/70	40, 80, 160	1.8
	50/50	40, 80, 160	1.4
	70/30	40, 80, 160	1.6
	90/10	5, 10, 20, 40, 80, 160	1.7
	97/3	40, 80, 160	1.8

TABLE 1. List of computer runs for one-dimensional normal shock waves in Ar–He mixtures

by collision with the wall and leaving the wall with a mean velocity according to the wall temperature (full accommodation, $\alpha = 1$). Close to the wall (i.e. up to about one mean free path from the wall) these decelerated gas particles accumulate and cause the forward bend of the density front close to the wall. The observation that this forward-bend part of the density front grows with increasing shock Mach number supports this explanation. This phenomenon was mentioned for the first time by Sichel (1962). He studied the problem of a shock wave close to a wall for weak shock waves with solutions of truncated Navier–Stokes equations.

5. Shock structure in inert-gas mixtures

The observed large gradients in the flow variables prompted the investigation of the shock structure close to a wall in binary gas mixtures (helium–argon). It was quickly found that the temperatures of both components do not relax to the common equilibrium value $(T-T_1)/(T_2-T_1) = 1$ downstream in the centre of the shock wave. After some trial simulation computer runs, done for the simpler model of a normal and undisturbed one-dimensional shock wave, it turned out to be a question of the number N of model gas particles per cell and component, put in at the beginning of

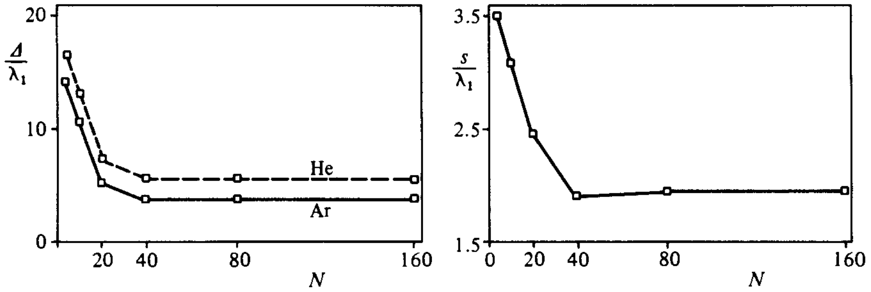

FIGURE 8. Dependence of the shock thickness Δ and the horizontal separation s at $(\rho-\rho_1)/(\rho_2-\rho_1) = 0.5$ on N (number of gas particles per cell and component). Simulation, 90% Ar–10% He mixture, $M_s = 3.5$.

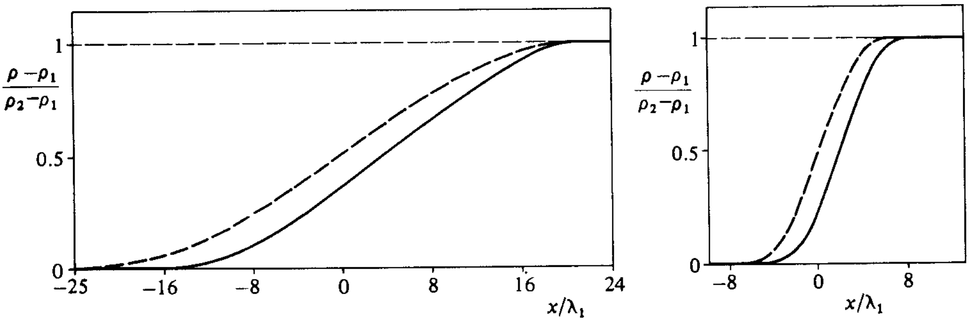

FIGURE 9. Density profiles for $N = 4$ and $N = 160$ (simulation), 10% Ar–90% He mixture: ——, argon; -----, helium; $M_s = 3.5$, rigid-sphere model.

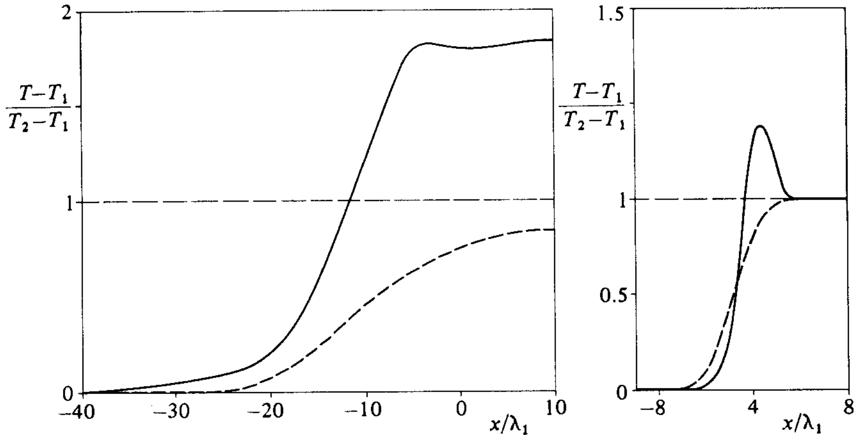

FIGURE 10. Temperature profiles for $N = 4$ and $N = 160$ (simulation), 10% Ar–90% He mixture: ——, argon; -----, helium; $M_s = 3.5$, rigid-sphere intermolecular-force potential.

a numerical simulation run (Schmidt & Wörner 1983; Wörner 1982). Results of systematic computer simulation runs (see table 1) show that the number N of gas particles per cell and component, up to a certain N, influences the calculated density, velocity and temperature profiles of the components in the shock wave. Figure 8 shows that $N \gtrsim 40$ gas particles are necessary to get an N-independent density profile.

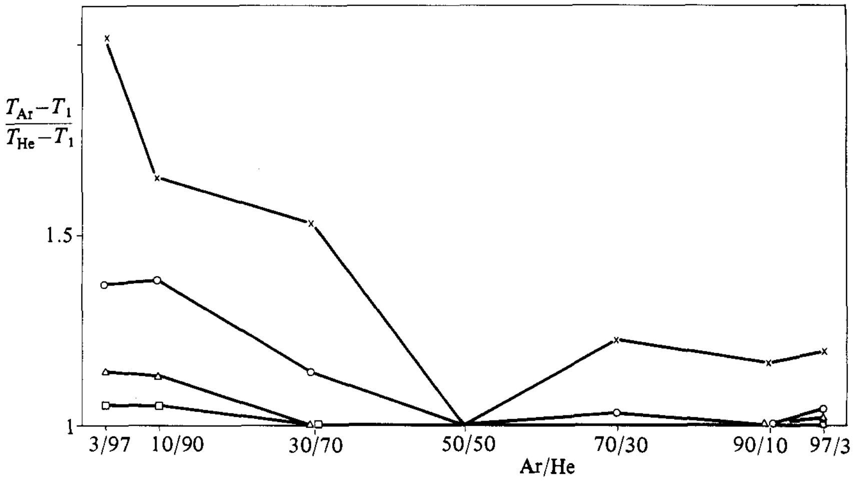

FIGURE 11. Particle-number N-dependence of the temperature relaxation downstream of the shock wave. Simulation calculation, rigid-sphere intermolecular-force model: ×, $N = 4$; ○, 20; △, 40; □, 80. $M_S = 3.5$.

Δ is the density-profile width between $(\rho-\rho_1)/(\rho_2-\rho_1) = 0.1$ and 0.9 and s is the horizontal separation at $(\rho-\rho_1)/(\rho_2-\rho_1) = 0.5$. For density profiles the influence of N is clearly visible in figure 9. The profiles have been calculated with $N = 4$ and $N = 160$. Much more sensitive to N are the temperature profiles (see figure 10). For $N = 160$ the temperature in the downstream part of the shock wave relaxes very fast from an argon temperature overshoot to the final equilibrium value $(T-T_1)/(T_2-T_1) = 1$. For $N = 4$ (figure 10, left graph) no relaxation is indicated. Unfortunately, temperatures can't be measured in a shock-tube experiment. Figure 11 shows the N-dependence of the temperature ratio $(T_{Ar}-T_1)/(T_{He}-T_1)$ downstream of the shock wave. For diluted mixtures of helium in argon, or even more for such mixtures of argon in helium, $N = 80$ is barely sufficient for a correct simulated temperature relaxation downstream of the shock wave. An exception is the mixture 50 % He–50 % Ar. Here the weighting factor, which models the mixture ratio, is unity. This gas mixture behaves more like a one-component gas, and therefore is less sensitive to N than the other mixtures.

6. Comparison of theoretical and experimental results

Accurate experimental results are needed to check the validity of the theoretical model and the numerical simulation method results. In figure 12 (Harnett & Muntz 1972; Goldman & Sirovich 1969; Sherman 1960), figure 13 (Harnett & Muntz 1972) and figure 14 (Center 1967), theoretical and experimental velocity, temperature and density profiles are compared for only a few typical results. The velocity and temperature measurements (figure 12 and 13) have been done in a stationary shock wave, generated in a supersonic low-density flow at the exit of a nozzle with the shock wave in front of a shock holder. The electron-beam-luminescence method has been applied here on a stationary shock wave to extract the bulk gas velocity, the local density and the local temperature from the measured velocity distribution of the electron beam excited and radiating gas particles (Harnett & Muntz 1972). In

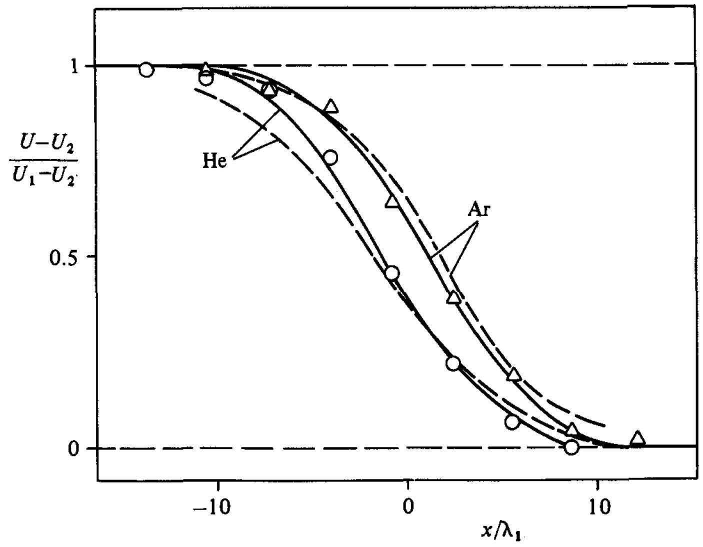

FIGURE 12. Comparison of velocity profiles: ○, He; △, Ar, experiment (Harnett & Muntz (1972); -----, theory (Sherman 1960; Goldman & Sirovich 1969); ——, simulation, 11.5% Ar–88.5% He, $M_s = 1.58$.

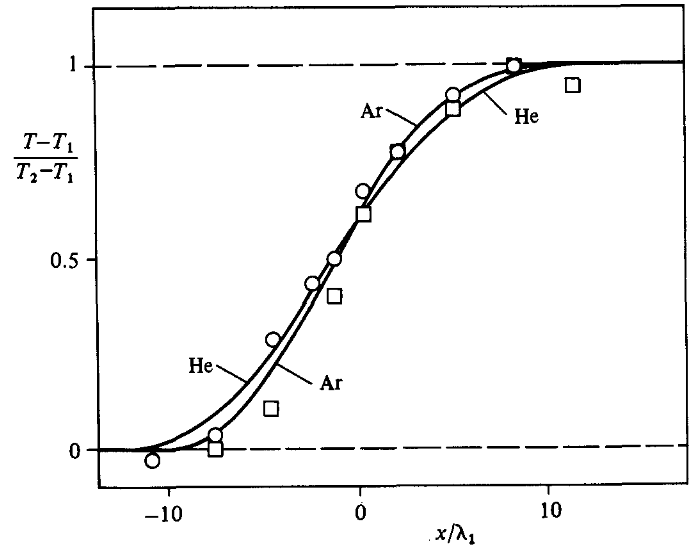

FIGURE 13. Comparison of temperature profiles: ○, He; □, Ar, experiment (Harnett & Muntz 1972); ——, simulation, 11.5% Ar–88.5% He, $M_s = 1.58$.

general, the numerical results, calculated with $N = 160$ particles per cell and component, are close to the experimental data.

A special case is the shock structure of a $M_s = 3.89$ shock wave in a 3% xenon–97% helium mixture (figure 15). The differences among the experimental data (Gmurczyk, Tarczynski & Walenta 1979), the results of a modified BGK model (Płatkowski 1979) and the results of the numerical simulation (Schmidt & Wörner 1983; Wörner 1982) are enormous. It is still an open question as to which result will be closest to the true density profiles.

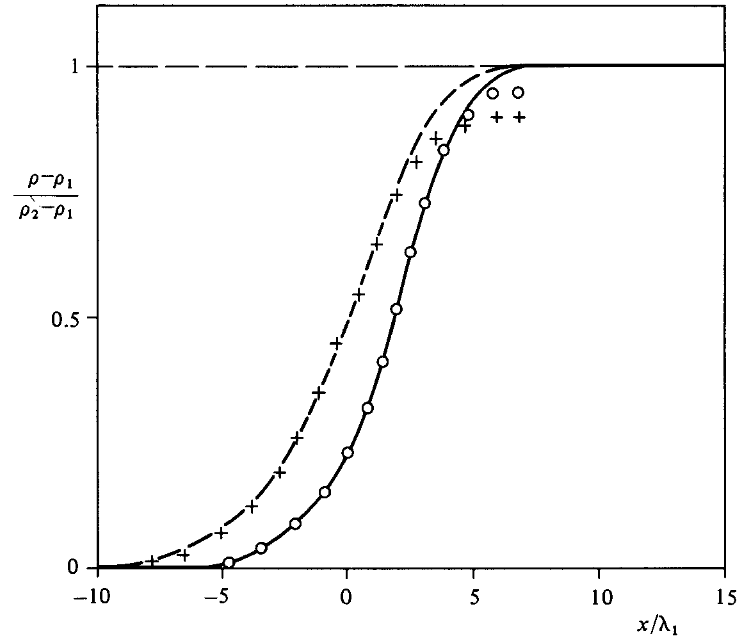

FIGURE 14. Comparison of density profiles: -----, He; ——, Ar simulation, + + + + +, He; ○○○○○, Ar experiment (Center 1967); 48 % Ar–52 % He, $M_s = 2.2$.

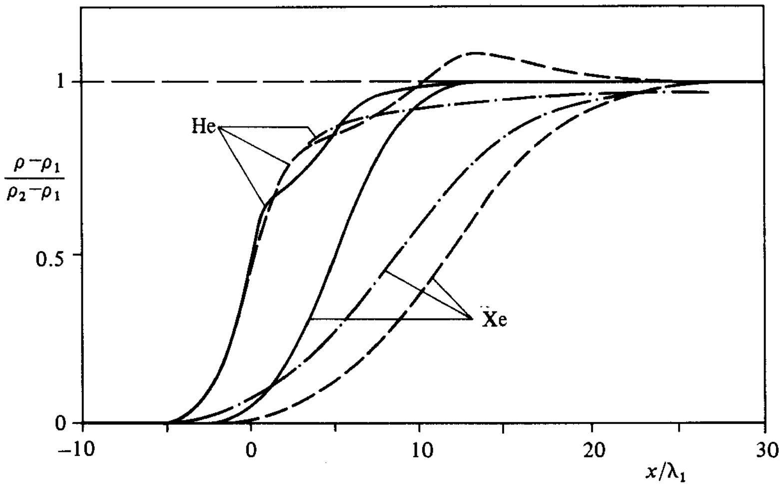

FIGURE 15. Density profiles: ——, simulation with $N = 160$; -----, experiment (Gmurczyk *et al.* 1979); —·—·—·, calculation (Płatkowski 1979); 3 % Xe–97 % He, $M_s = 3.89$.

The dent in the helium density profile is curious. For the simulation method the dent becomes visible at $N \gtrsim 60$ particles per cell and component. For $N = 10$ the dent does not appear (see figure 16), and moreover the density profiles are less inclined. The dent becomes less pronounced with increasing concentration of xenon and disappears at 9 % Xe–91 % He.

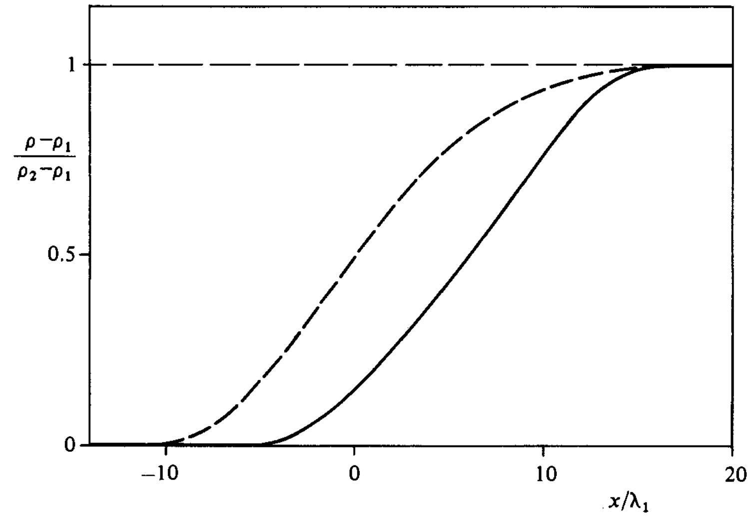

FIGURE 16. Density profiles for a 3 % Xe–97 % He mixture: ——, Xe; -----, He; simulation, $N = 10$, $M_s = 3.89$.

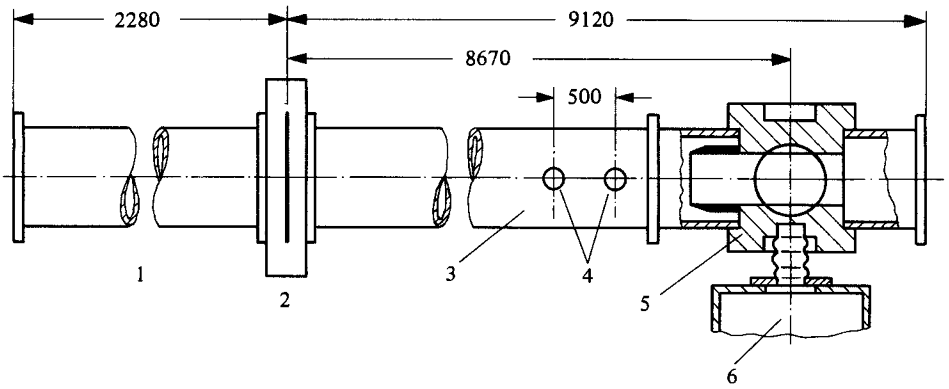

FIGURE 17. Dimensions of the shock tube, inner diameter 150 mm, lengths in mm: 1, driver; 2, diaphragm; 3, driven section; 4, thin-film gauge heads; 5, test chamber; 6, electron-beam chamber.

7. Application of the electron-beam-luminescence method in a shock tube

In order to obtain some experience with the electron-beam-luminescence method for measuring partial densities of the components of a gas mixture (Muntz 1968), this method was applied to shock-structure measurements in a 50 % Ar–50 % He mixture in a shock tube. The volume of density measurement was in the centre of the test section.

For the electron-beam-luminescence method, the test section, mentioned in §4, has been replaced by a similar one of 90 × 90 mm cross-section, but with a hole of 0.9 mm diameter in the bottom for admission of the electron beam and a beam collector in the opposite (top) wall (figure 17). Figure 18 is the wiring plan for the signal-recording devices (waveform recorder Biomation 8100) and the arrangements to protect the electron beam-gun cathode after the passage of the shock wave from too high pressure

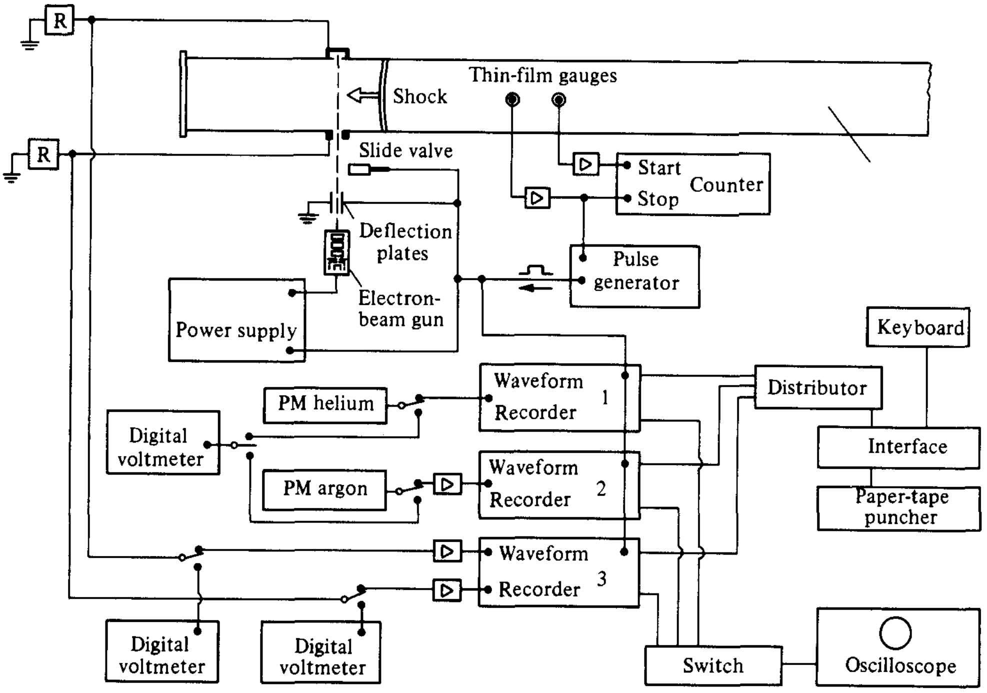

FIGURE 18. Wiring plan for the electron-beam-luminescence method to measure the partial density of helium and argon.

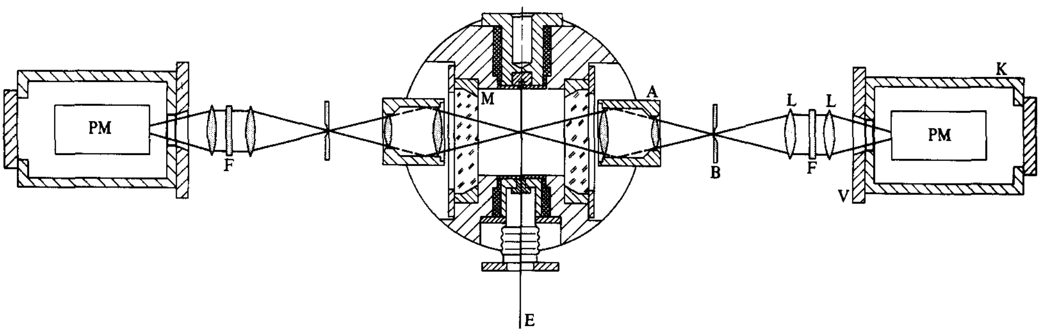

Figure 19. Optical arrangement for the luminescence method. A, photo lens $f = 50$ mm; B, screen with hole 0.9 mm; E, electron beam; F, light filter; K, cooling chamber; L, lens; M, test section; PM, photomultiplier; V, shutter.

and from poisoning (cut-off of cathode-heating current and beam high voltage, separation of the gun chamber by a slide valve).

Figure 19 shows the optical arrangement to record the light coming from the electron-beam-excited gas at the centre of the test chamber. The region of measurement is projected by a photo lens ($f = 50$ mm, aperture 1 : 1) with a scale of 1 : 1 on the hole of 0.9 mm diameter in the screen B. The hole is now the light source for the optics behind the screen (lenses L, filter F, photomultiplier PM).

The main problem of this method to measure partial densities is here the low intensity of the argon spectrum line ($\lambda_{\mathrm{Ar}} = 4610$ Å). This line is one of the brightest

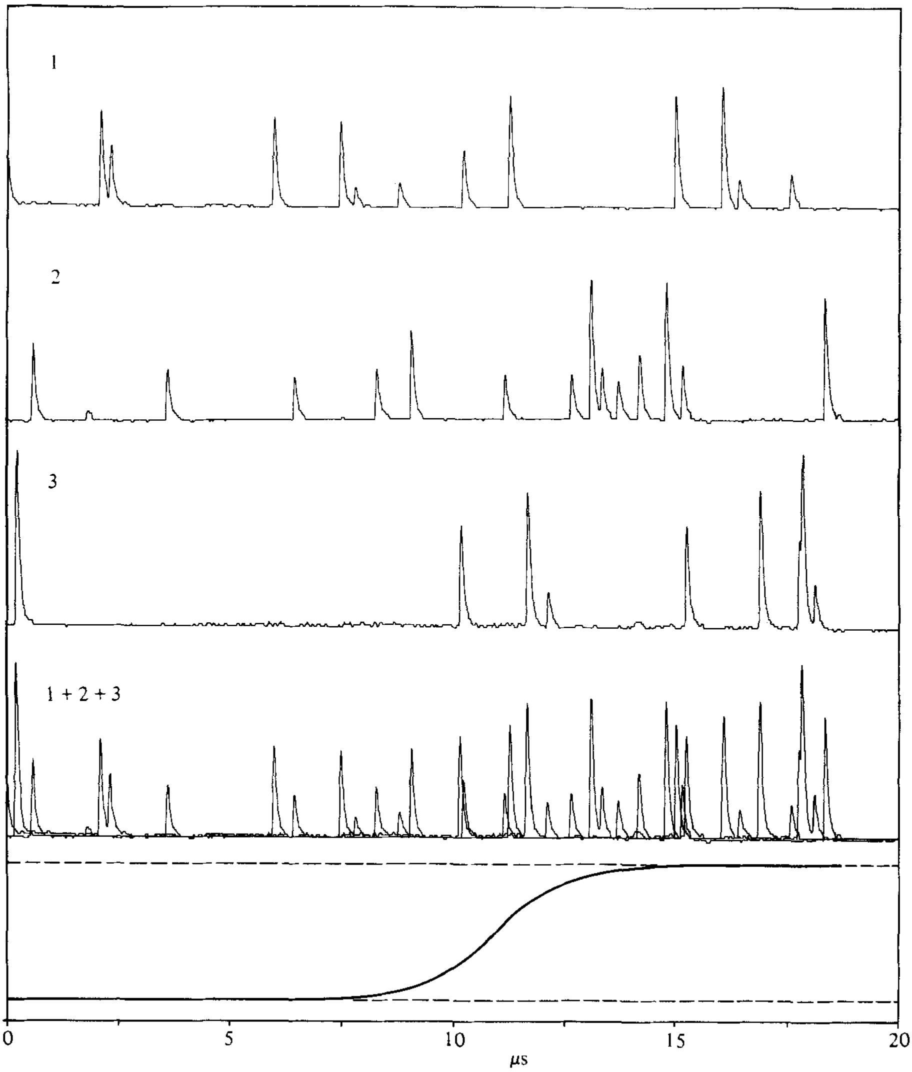

FIGURE 20. Argon photomultiplier signals and their superposition.

in the visible spectrum of argon, but is very weak in absolute terms. A very sensitive photomultiplier (RCA C 31034 A-02) was used to record this weak signal. The helium line used ($\lambda_{He} = 5016$ Å), is about ten times as bright at the same gas density and beam current. The helium signal was recorded with a less sensitive photomultiplier (RCA 8575).

The low density ρ_1 ($p_1 = 13.32$ N/m^2, $T_1 \approx 293$ K), required to spread the shock-wave region for structure measurements, lowered the output for the component density measurements to less than one photon per microsecond for argon. The single photons are registered with about 30 % efficiency and appear as 20–40 ns current pulses at the anodes of the photomultipliers (see figures 20 and 21). To obtain an acceptable scatter for the experimental results for a 50 % He–50 % Ar mixture, the data of forty almost identical runs are superimposed for argon and about six for helium. The pulse distributions of the superimposed experimental records are

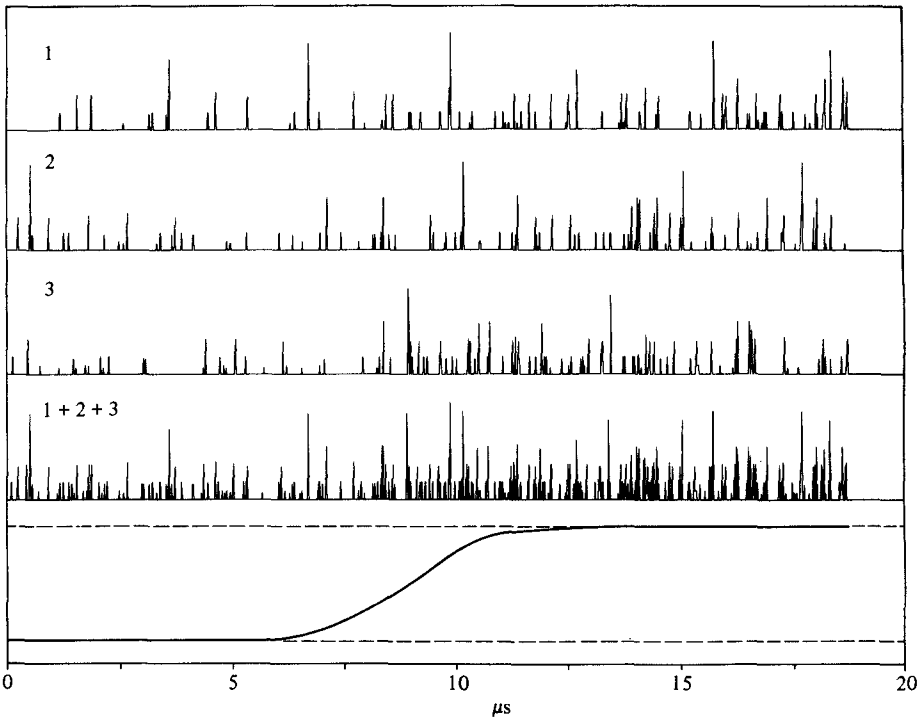

FIGURE 21. Helium photomultiplier signals and their superposition.

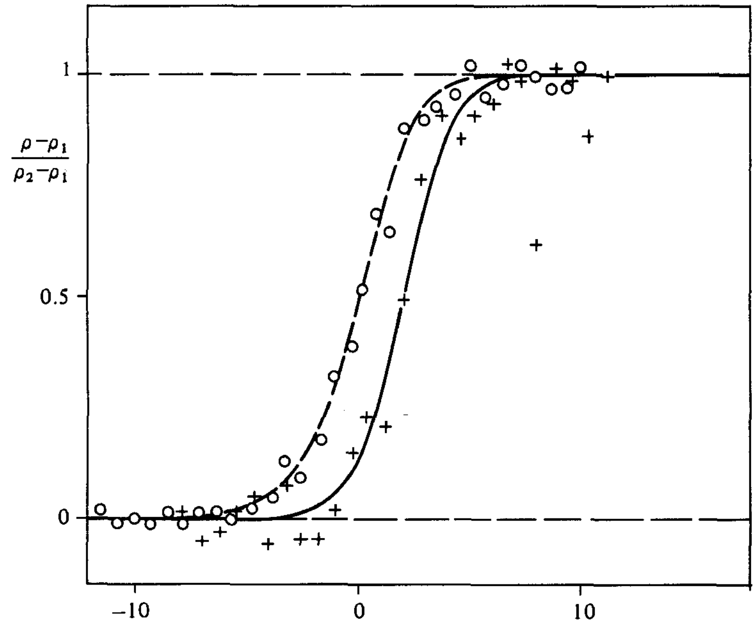

FIGURE 22. Comparison of measured and calculated density profiles: ——, Ar; -----, He simulation; + + + + +, Ar; ○○○○○, He experiment; 50% Ar–50% He, $M_s = 3.5$.

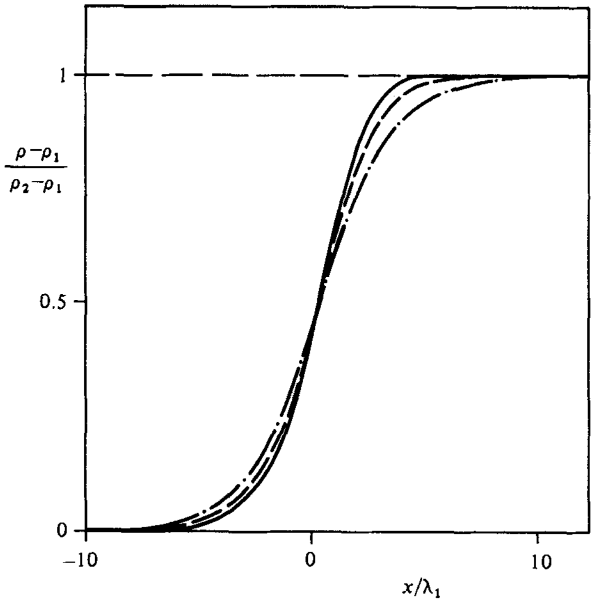

FIGURE 23. Gas-mixture density profiles (He + Ar); –•–•–, experiment; -----, experiment, curvature-corrected; ——, simulation, $N = 160$; 50% Ar–50% He, $M_s = 3.5$.

converted to the component partial-density profiles by means of accurate calibration curves. Figure 22 shows the result of such a data reduction. The experimental data are compared with the corresponding results of the numerical simulation method. Except for two far-off argon points, the agreement is good.

The electron beam attenuation over the full 90 mm of the test section provided, in connection with a calibration, the average density profile of the binary mixture (50% He–50% Ar). The measured density profile is disturbed by the shock-wave curvature and by shear-layer effects close to the test-chamber windows. An approximate curvature correction is possible with a theoretical curvature estimation (DeBoer 1963). Except for a very limited region near the walls, the theoretical curvature is close to the measured one (Schmidt 1976). Figure 23 shows the effect of the curvature correction. The average mixture density profile becomes steeper and moves closer to the numerical-simulation result.

8. Two-dimensional shock structure close to a wall in a binary inert gas mixture (He–Ar)

For the simulation of the two-dimensional flow field of a shock wave close to a wall in a binary gas mixture, a two-dimensional model, as shown in figure 2, has been used. One important difference to the pure-gas simulation calculation is the requirement of more gas particles per cell and component, N, at the beginning of a simulation run. Core storage capacity and the time needed for one simulation run on the computers used (Burroughs B 7700 of the computer centre, University of Karlsruhe, and IBM 370/168 of the computer centre, University of Heidelberg) limited the number of gas particles to $N \lesssim 40$. This is, as demonstrated in §5, barely sufficient for results to be independent of N.

The numerical simulation method results for three different mixtures are shown

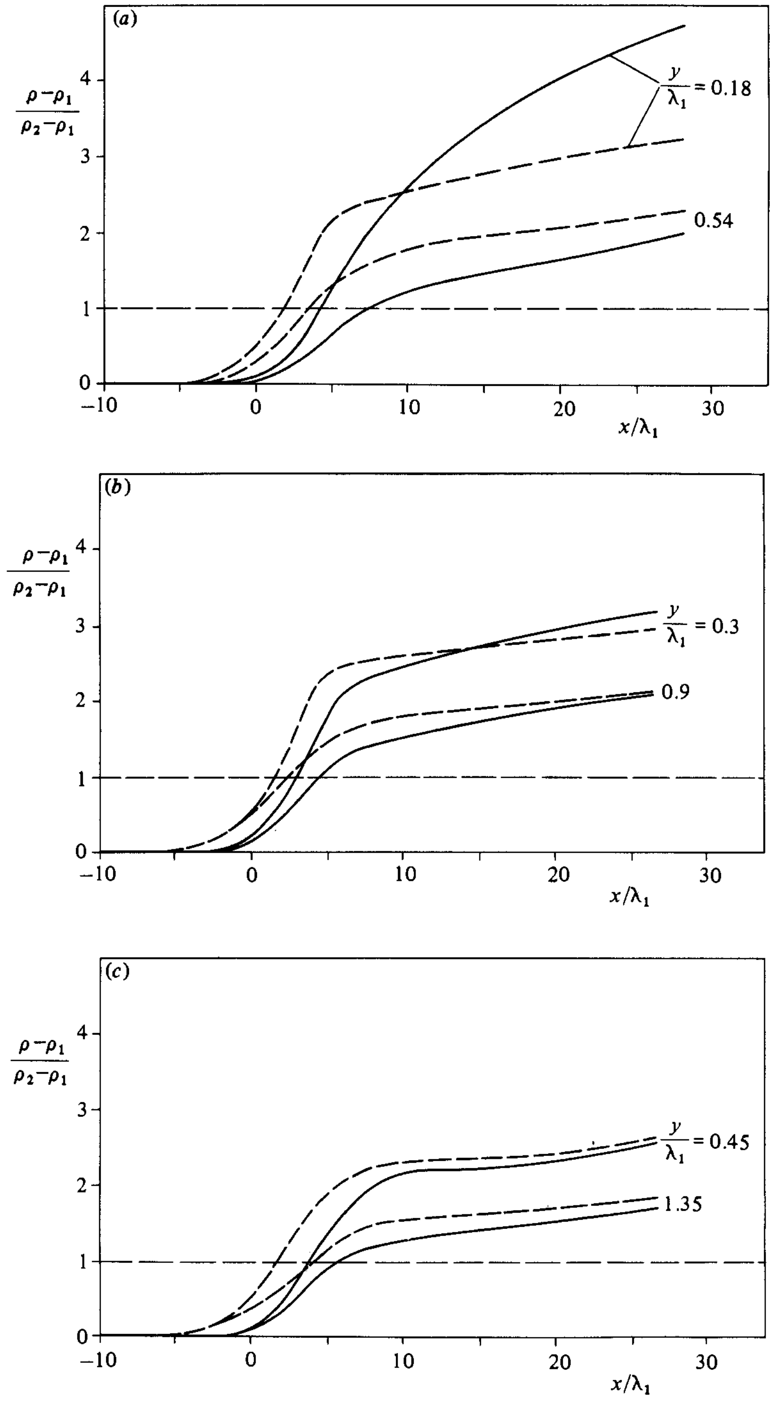

FIGURE 24. Density profiles of a shock wave close to a wall: ——, Ar; - - - - -, He simulation, $M_s = 3.5$. (*a*) 3% Ar–97% He, $H/\lambda_1 = 64.2$, $\lambda_1 = 1.402$ mm; (*b*) 50% Ar–50% He, $H/\lambda_1 = 108.3$, $\lambda_1 = 0.831$ mm; (*c*) 90% Ar–10% He, $H/\lambda_1 = 161.6$, $\lambda_1 = 0.557$ mm.

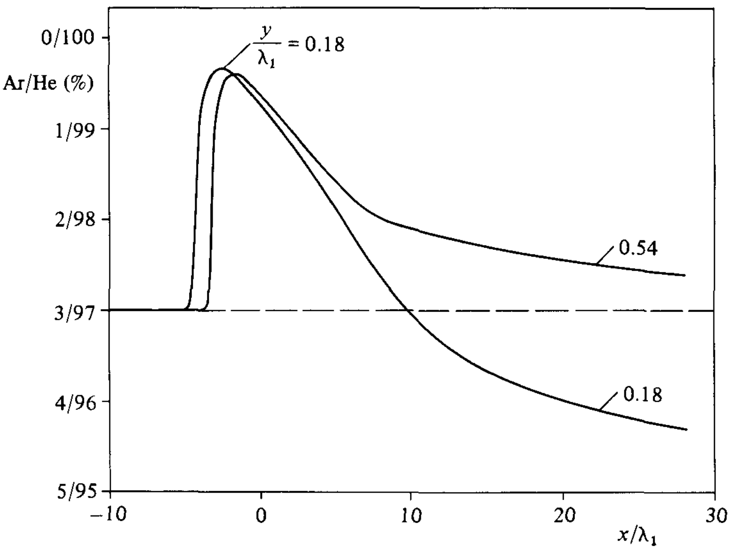

FIGURE 25. Change of the mixture ratio in the region close to the wall for a 3 % Ar–97 % He mixture.

Mixture ratio Ar/He (%/%)	Overall number of particles at $t = 0$ per component	Average computing time per simulation run (h)	λ_1 (mm)
3/97	47600	7.5	1.402
10/90	44800	6.3	1.299
50/50	43680	4.5	0.831
90/10	42280	4.5	0.557
97/3	42280	4.8	0.529

Mixture ratio Ar/He (%/%)	Cell centre (y/λ_1)/cell height (λ_1)						
3/97	0.18/0.36	0.54/0.36	1.07/0.71	2.14/1.43	4.28/2.85	9.98/8.56	23.18/17.83
10/90	0.19/0.38	0.58/0.38	1.15/0.77	2.31/1.54	4.62/3.08	10.78/9.24	25.02/19.25
50/50	0.30/0.60	0.90/0.60	1.80/1.20	3.61/2.41	7.22/4.81	16.84/14.43	39.10/30.07
90/10	0.45/0.90	1.35/0.90	2.69/1.80	5.39/3.59	10.77/7.18	25.13/21.54	58.35/44.88
94/3	0.47/0.95	1.42/0.95	2.84/1.89	5.67/3.78	11.35/7.56	26.48/22.69	61.46/47.28
	Cell centre (mm)/cell height (mm) (kept constant for all mixture ratios)						
	0.25/0.5	0.75/0.5	1.5/1.0	3.0/2.0	6.0/4.0	14.0/12.0	32.5/25.0

TABLE 2. List of computer runs for two-dimensional shock waves in Ar–He mixtures; $M_s = 3.5$, test-section height $H = 90$ mm

in figures 24(*a–c*). Since here the cell height Δy is considered a constant, the values of $\Delta y/\lambda_1$ are different on the three figures. For gas mixtures, λ_1 is a function of the mixture ratio, too. This makes it difficult to compare the computed density profiles of the figures 24(*a–c*) with each other. To take Δy to be a constant was done with respect to the experiment. The size of the volume of measurement was constant. To compare computed simulation results that are an average over Δy with measured data, Δy should be the height of the volume of measurement. Figure 25 shows the calculated change of the mixture ratio in the region close to the wall for a 3% Ar–97% He mixture ($y/\lambda_1 = 0.18$, $y/\lambda_1 = 0.54$). The mixture ratio shifts from a dilution of argon in the shock wave to a concentration of argon at the bottom of the shear layer. Because of the computing time needed to reduce the scattering of the results to an acceptable level, only the density profiles for a limited number of mixtures and for one shock Mach number ($M_S = 3.5$) have been computed (see table 2).

9. Partial density measurements in a shock wave close to a wall in a binary gas mixture

Extending the electron beam luminescence method to do partial density measurements in a shock wave close to a wall in helium-argon mixtures, it turned out that the electron beam has to be about ten to fifteen times more powerful as that one, used for the structure measurements in an undisturbed shock wave in a 50% argon–50% helium gas mixture (§7). The modified television picture tube guns used don't allow a beam current of more than 0.4 mA.

10. Conclusions

Large gradients in the flow variables have been found in the region where a shock wave touches a wall. The flow becomes two-dimensional in this region. The very strong influence of the wall is limited to not much more than one mean free path λ_1 (of the state '1' ahead of the shock wave) from the wall. Numerical results, computed with the direct-simulation Monte Carlo method, are compared with experimental data that are reduced from signals of a multibeam laser differential interferometer. The agreement between the results is good in some places but poor in others. The agreement can be improved for strong shock waves ($M_S \gtrsim 6$) by lowering the accommodation coefficient α from $\alpha = 1$ (full accommodation) to a value $\alpha < 1$. The stronger the shock wave the more α drops below unity. For weaker shock waves ($M_S \lesssim 4$), full accommodation ($\alpha = 1$) is indicated. The differences between measured and calculated density profiles for $M_S \lesssim 4$ will become less by applying a Lennard–Jones intermolecular-force potential with a softer repulsive term $(\sigma/r)^\nu$ with $\nu < 12$ but keeping the attractive term $(\sigma/r)^6$ unchanged.

For reasons not known the BGK model density profiles deviate already inside of the shock wave considerably from the experimental profiles and from the simulation calculation results (figure 5). Downstream of the shock wave, the BGK density profiles level off to a constant density, because the influence of the boundary layer has not been taken into consideration.

The influence of the wall material is demonstrated experimentally by the exchange of the aluminium plate at the bottom of the test section with a glass or a PVC (polyvinyl-chloride) plate. There are larger differences in the density profiles close to the wall between glass and aluminium than between glass and PVC (figure 6). Responsible for these differences in accommodation seems to be rather the heat conduction of the wall material than the surface condition (superfinished aluminium plate, glass and PVC surface are smooth by fabrication process; surfaces cleaned for use in high vacuum).

The forward bend of the density shock wave front at the wall is real and can be explained by the accumulation of fast (hot) gas particles, coming from a region of higher temperature downstream of the density front and collide with the wall under full accommodation ($\alpha = 1$) or collide with gas particles coming direct from the wall. This forward bend of the density shock front was mentioned first by Sichel (1962).

For the application of the numerical-simulation method it is important, especially in the case of gas mixtures, to put a sufficient number of gas particles at the start into each simulation cell. By a systematic change of the parameters, mixture ratio and shock Mach number, it is found that about 40–80 gas particles per cell are needed to get results that are independent of the number of gas particles per cell.

For the shock-structure density measurements in gas mixtures, the electron-beam-luminescence method has been applied to a $M_s = 3.5$ normal shock wave in a 50 % He–50 % Ar mixture. The density estimation for the very weak signals was done by counting pulses-per-microseconds. The scattering was reduced by superimposing the pulse distributions of forty almost identical runs for the argon signal and of about six runs for the helium signal. The pulses per microsecond are converted to component density by calibration. The agreement between the measured component densities and the calculated ones is good.

No measurements have been done in the two-dimensional flow field of a shock wave close to a wall in a binary gas mixture. The electron beam guns used (television picture tube electron-beam guns) are not powerful enough to get a sufficient pulse density per microsecond for argon, especially with the argon being diluted by helium to less than 50 %.

The financial support of the project by the D.F.G. (Deutsche Forschungsgemeinschaft, Bonn–Bad Godesberg, W. Germany) is gratefully acknowledged.

REFERENCES

Bird, G. A. 1976 *Molecular Gas Dynamics*. Clarendon.

Center, R. S. 1967 *Phys. Fluids* **10**, 1777–1784.

DeBoer, P. C. T. 1963 *Phys. Fluids* **6**, 962–971.

Gajewski, P. & Schmidt, B. 1980 Paper presented at Euromech 125, Oxford.

Gmurczyk, M., Tarczynski, M. & Walenta, Z. A. 1979 In *Rarefied Gas Dynamics*, vol. 1, pp. 333–340.

Goldman, E. & Sirovich, L. 1969 *J. Fluid Mech.* **35**, 575–597.

Harnett, L. N. & Muntz, E. P. 1972 *Phys. Fluids* **15**, 565–572.

Muntz, E. P. 1968 *AGARDograph* 132.

Płatkowski, T. 1979 In *Rarefied Gas Dynamics*, vol. 1, pp. 323–332.

Schmidt, B. 1976 *Arch. Mech.* **28**, 809–815.

Schmidt, B. & Wörner, M. 1982 *Arch. Mech.* **34**, 325–331.

Schmidt, B. & Wörner, M. 1983 *Acta Mech.* **46**, 49–55.

Seiler, F. 1980 Dissertation, Karlsruhe (in German).

SEILER, F. & SCHMIDT, B. 1979 In *Recent Developments in Theoretical and Experimental Fluid Mechanics*, pp. 208–213. Springer.

SEILER, F. & SCHMIDT, B. 1981 *Prog. Astronaut. Aeronaut.* **74**, 1094–1104.

SHERMAN, F. S. 1960 *J. Fluid Mech.* **8**, 465–480.

SICHEL, M. 1962 *Phys. Fluids* **5**, 1168–1180.

WÖRNER, M. 1982 Dissertation, Karlsruhe (in German).